IJE TRANSACTIONS B: Applications Vol. 29, No. 5, (May 2016) 669-676

International Journal of Engineering

Journal Homepage: www.ije.ir

Effect of Welding Heat Input on the Intermetallic Compound Layer and Mechanical Properties in Arc Welding-brazing Dissimilar Joining of Aluminum Alloy to Galvanized Steel

M. Zarouni*, R. Eslami-Farsani

Faculty of Materials Science and Engineering, K. N. Toosi University of Technology, Tehran, Iran

P A P E R I N F O

Paper history:
Received 02 November 2015
Received in revised form 13 February 2016
Accepted 04 March 2016

Keywords:
Arc Welding-brazing
Numerical Simulation
Dissimilar Alloy
Intermetallic Compound Layer

A B S T R A C T

The effect of weld heat input on the formation of intermetallic compound (IMCs) layer during arc welding–brazing of aluminium and steel dissimilar alloys was investigated through both finite element method (FEM) numerical simulations and experimental measurements. The results of FEM analysis as well as welding experiments indicated that increasing weld heat input increases the thickness of IMCs layer. The thickness of IMCs layers, as calculated from FEM simulations, was approximately equal to that measured from microstructural images in the range of 2-6 μm. The tensile strength of arc welding–brazing joints was dependent on the thickness of IMCs layer and spreading of molten weld metal on the surfaces of steel sheet. The highest mechanical strength of 120 MPa was obtained in the optimized heat input of 420 J/mm. The presence of the Si element in the Al-5Si filler metal led to IMCs layer with the composition of $Fe(Al,Si)_3$ phase in side of the steel and $Al_{7.2}Fe_{1.6}Si$ phase in side of the weld seam.

***doi**: 10.5829/idosi.ije.2016.29.05b.11*

1. INTRODUCTION

There has been a growing demand for hybrid structures of aluminium alloy and steel in the automotive, aerospace, and marine industries to reduce pollution and save energy by reducing the vehicle weight. To achieve such structures, joining aluminium with steel is unavoidable. However, direct arc welding of aluminium to steel is very difficult because of the large differences between their thermo-physical and thermo-chemical properties and the formation of a large amount of brittle IMCs in the interface steel/weld seam with plate-like morphology [1, 2].

The mechanical joining processes, including friction stir welding and ultrasonic welding, were investigated to make sound joints. However, the dimension and configuration of the joints have restricted these methods [3-5].

*Corresponding Author Email: *9005494@gmail.com* (M. Zarooni)

Other processes such as the explosive welding, adhesive bonding, and laser welding-brazing can also be used [6, 7].The arc welding–brazing, as a low cost and compatible joining technique, has a high potential to join aluminium to steel. In this process, aluminium is melted and mixed with molten filler wire, but steel is not melted and only wetted by molten metal; thus, this process is a hybrid of welding in aluminium side and brazing in steel side [8, 9].

Su et al. [10] investigated the effect of alloy elements (Mg and Si) on thickness, morphology, and composition of IMCs layer in joints made with alternate-current double pulse gas metal arc welding method. It was found that the Mg content could not restrain the growth of IMCs layer, resulting in poor mechanical properties of the joint, while the addition of Si could reduce the thickness of Fe2Al5 sub-layer and the mechanical properties of joints were improved with increasing Si content in the IMCs layer.

Dong et al. [11] lap-joined 5A02-H34 (AA 5052-H34, ASTM B209-5052) aluminium alloy to uncoated

Please cite this article as: M. Zarouni, R. Eslami-Farsani , Effect of Welding Heat Input on the Intermetallic Compound Layer and Mechanical Properties in Arc Welding-brazing Dissimilar Joining of Aluminum Alloy to Galvanized Steel, International Journal of Engineering (IJE), TRANSACTIONS B: Applications Vol. 29, No. 5, (May 2016) 669-676

Q235B (ASTM A36) carbon steel by gas tungsten arc welding process with Zn-15Al flux-cored filler wire. They detected a Fe-rich layer detached from the interfacial layer. Moreover, they reported that the PWHT improved the joint strength from 111 MPa to 150 MPa by relieving thermal and residual stresses in the joint.

Chen et al. [12] simulated the laser welding–brazing of aluminium to titanium by finite element method with MARC software. They investigated the effect of laser spot mode on the characteristics of the thermal cycles and reported that rectangular spot laser welding–brazing could obtain more uniform interfacial reaction than circular spot mode. Simulation of tungsten inert gas (TIG) welding-brazing of aluminium to steel and identification of the influence of the heat input on the characteristics of the thermal cycle and thickness of IMCs layer, has not been conducted yet.

The growth of the IMCs layer is controlled by diffusion of solid iron in molten aluminium. In order to reduce the thickness of IMCs layer, temperature history near the bond region should be controlled. The factors such as welding speed and using a heat sink can be effective to control heat flow and thermal history during TIG welding-brazing [13, 14].

The weld heat input is calculated using Equation (1):

$$Q = \frac{\eta UI}{v} \quad (1)$$

In Equation (1), η=0.5 is the arc efficiency, U is the voltage, I is current and v is the welding speed [15].

The objective of this paper was to investigate the effect of heat input caused by TIG welding source on main parameters effective on the joint strength, i.e. thickness of IMCs layers formed in the interface of weld seam/steel and spreading of molten filler wire on the surface of steel sheet. In this study, the experimental TIG welding-brazing of 5083 aluminium alloy to galvanised steel with Al-5Si filler wire was conducted. Moreover, the thermal analys of the joining process by FEM simulation was carried out. The ABAQUS software was applied for FEM numerical simulation. IMCs layers were identified by both FEM numerical simulation and microscopy images.

2. MATERIAL AND EXPERIMENTAL

The materials used in this study were AL5083 and galvanised steel[2] sheets with the thickness of 3 mm and 2 mm, respectively. These materials were butt welded by TIG welding brazing method with an Al-5Si filler wire having the diameter of 2.5 mm. Table 1 shows the chemical composition of the sheets and filler wire. The non-corrosive flux with main compositions Nocolok flux ($KAlF_4$ and K_3AlF_6 eutectic) was dissolved in acetone. This suspension, with the thickness of 0.5 mm, was homogenously smeared on both front and back faces of the steel and in close contact with the groove.The sheets were cut in size of 200×100 mm^2 and were cleaned by abrasive paper and acetone.

The joint pattern used was a butt joint with a dual characteristic including a bevel angle of 30° in aluminium alloy side and semicircular pattern in steel side. The joint pattern and the joining process are shown in Figure 1 schematically. A copper backing plate with the dimension of 210×210×10 mm^3 and a shaped groove in the size of 10×0.5 mm^2 on its front face was used.

The joining process was carried out using TECHNO TIG 250-P welding source. The type of welding current used was AC. Four groups of welding parameters with different heat inputs were used, as shown in Table 2.

Typical transverse sections of the joints were cut and mounted in self-setting epoxy resin in as-clamped condition. For metallography treatment, the samples were polished to a mirror-like surface and etched with keller's reagent (1ml HF+1.5 ml HCl+2.5 ml HNO_3-+95ml H_2O) for 3-5 s. The microstructures of the joints were observed using optical microscopy and SEM[3].

To measure the compositions of IMCs layer, the energy dispersive spectrometer was used. In addition, the samples of tensile test were cut and the joints tensile strength was measured.

3. FEM NUMERICAL SIMULATION

The ABAQUS software[4] was used to determine the temperature cycles in the interface of steel/weld seam. Due to different materials and dimensions of components, the whole model of butt-welded components, according to experimental dimensions, was built.

Because of the severe gradients of temperature adjacent of the weld seam, a non-uniform meshing was used and by keeping away from centerline, the size of elements were increased [16]. The linear hexahedral elements (DC3D8), were used. The total number of nodes and elements was 24380, 15530, respectively.

The governing equation for transient non-linear heat transfer analysis is:

$$\frac{\partial}{\partial x}\left(k_x \frac{\partial T}{\partial x}\right)+\frac{\partial}{\partial y}\left(k_y \frac{\partial T}{\partial y}\right)+\frac{\partial}{\partial z}\left(k_z \frac{\partial T}{\partial z}\right) +Q = \rho C \frac{\partial T}{\partial t} \quad (2)$$

[1-] ASTM A653, Designation: CS type B

[3] - SEM MAG: 2.00kx, WD:23.75mm, SEM HV:15.00kv, Det:BSE Detector, Vac:HiVac

[4]- ABAQUS 6.11-PR3

where, k_x, k_y, k_z are the thermal conductivities in the x, y and z directions respectively, T is the current temperature, Q is the heat generation, ρ is the density, C is the specific heat capacity and t is the time, respectively. General solution of Equation (2) is obtained introducing the initial and boundary conditions, as follows:

❖ Initial condition:

$$T(x,y,z,0)=T_0(x,y,z) \tag{3}$$

❖ Boundary conditions:

$$\left(k_x\frac{\partial T}{\partial x}N_x+k_y\frac{\partial T}{\partial y}N_y+k_z\frac{\partial T}{\partial z}Nz\right)+q_s +h_c(T-T_\infty)+h_{r(T-T_r)}=0 \tag{4}$$

where, N_x, N_y, N_z are the direction cosine normal to the boundary, h_c and h_r are the convection and radiation heat transfer coefficients respectively, q_s is the boundary heat flux and T_r is the temperature of radiation heat source and T_∞ is the surrounding temperature.

Besides, the uniform heat flux was distributed on the weld elements, calculated by Equation (5):

$$q=\frac{\eta UI}{V_H} \tag{5}$$

In Equation (5), η=0.5 is the arc efficiency, U is the voltage, I is current and V_H is the volume of the activated weld element of seam [17].

In this study, to consider heat losses and simulate the weld cooling, the combined heat transfer coefficients of material from Equation (6) (Newton's law of cooling) were calculated. The values of 25, 8 and 53 W/m^{2}K were calculated for 5083 aluminium alloy, galvanised-steel and copper backing plate, respectively.

$$q_{loss}=h\times A\times(T-T_{amb}) \tag{6}$$

where q_{loss} is the loosed power from the outer surface, h is the combined heat transfer coefficient , T_{amb} is the ambient temperature, T is average surface temperature, and A is the area of surfaces [18].

In this study, the most important thermal and mechanical properties of 5083 aluminium alloy such as thermal conductivity, specific heat, yield stress, and density were assumed to be temperature dependent [19].

In addition, other properties such as Poisson's ratio, thermal expansion coefficient, latent heat, solidus and liquidus temperatures were assumed to be constant and temperature independent.The thermal and mechanical properties of galvanised steel and Al-5Si filler wire were considered constant [20, 21].

TABLE 1. Chemical compositions of 5083 aluminium alloy, galvanised steel and filler wire (weight percent %)

	Fe	Mn	Si	Ni	Cr	Al	Mg	C	P	S	Cu	Zn
AL 5083	0.25	0.3	0.29	0.033	0.136	Bal	3.95	0	0	0	0	0
Galvanized steel	99.2	0.38	0.015	0.059	0	0	0	0.073	0.017	0.02	0	0
AL-5Si	0.8	0.5	4.5-5	0	0	Bal	0.5	0	0	0	0.3	0.1

TABLE 2. The welding parameters

Sample number	Welding current (A)	Welding voltage (V)	Welding speed (mm/s)	Weld heat input (J/mm)
1	120	11	2.67	247.5
2	140	12	2.25	373.3
3	150	14	2.5	420
4	155	15	2.52	461.3

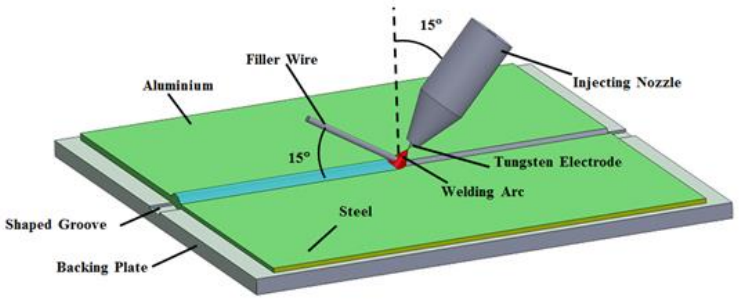

Figure 1. Scheme of joining process and joint pattern

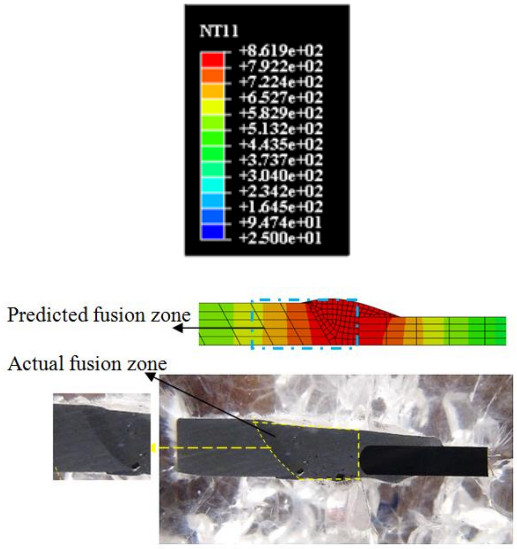

Figure 2. Comparison of the predicted and actual fusion zones in 420 J/mm heat input

It should be noted that to simulate the weld metal deposition, the element birth and death technique was used [22, 23]. In this technique, the weld seam is divided to the elements that will birth in the later stages of the analysis. First, the uniform heat flux is applied on the initial element and other elements are deactivated. Similarly, other elements are activated and cooled as long as weld metal which is deposited completely.

To verify the present FE method, the half width of the predicted and actual fusion zones according to the same parameters, were compared (Figure 2).

It is clear that the mass of the predicted fusion zone agrees with mass of the actual weld. Therefore, the FE program developed here is proved right, and it can be used for analysis in the butt welded joints.

4. RESULTS AND DISCUSSION

4. 1. Microstructure of the Joints Figure 3 shows the optical images from the cross-section of butt joints in interface areas between steel and weld seam.

As can be clearly seen, the increase of the weld heat input enhanced the IMCs layer thickness. The thicknesses of IMCs layers in whole set welding parameters was 2-6 µm, which was less than the maximum critical value of 10 µm, as shown in Figure 3. Moreover, the thickness of IMCs layer along interface in sample four was equal, whereas it was inhomogeneous with ragged surface in other samples.

Weld heat input and thermal conductivity rate the influencial contribution of the main factors, which are the molten time range and average diffusion coefficient, to the growth of IMCs layer [14, 24]. Utilizing copper backing block with high thermal conductivity and selecting optimized welding parameters repressed the growth of IMCs layer, and consequently increased the joint strength.

Due to the proximity of the weld heat input values of (2-4) samples, the IMCs thickness and weld seam dendritic microstructure of these samples did not show a large difference, as shown in Figure 3. It may be noted that the non-uniform thermal cycles along the interface of steel/weld seam caused the non-homogeneity of IMCs layers.

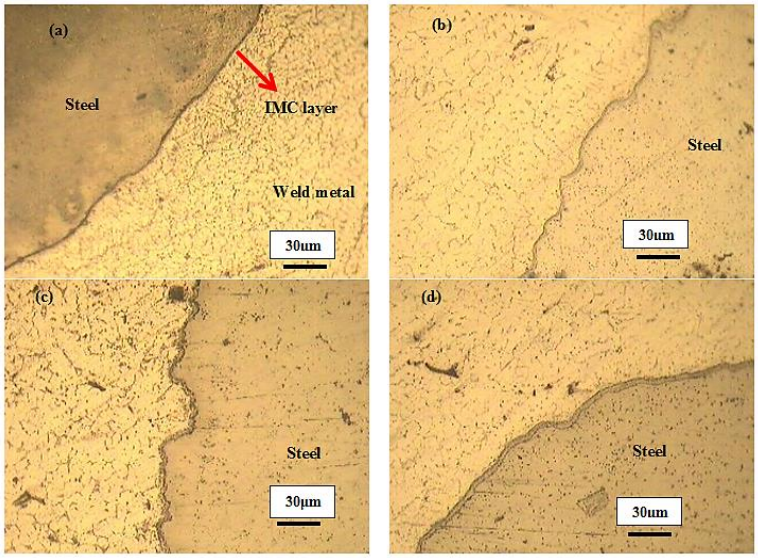

Figure 3. Optical microscopy images of the interface between steel and weld seam for different heat inputs: a 247.5 J/mm; b 373.3 J/mm; c 420 J/mm; and d 461.3 J/mm

Figure 4 shows the SEM image of the interface between steel and weld seam, related to the sample three. The brittle IMCs layer with plate-like morphology was formed in the interface of the steel and weld seam, as shown in Figure 4. Moreover, the intermetallic compounds with needle-like morphology in weld seam close to the interface were observed. Figure 5 shows the isothermal section of the Al–Fe–Si ternary phase diagram. Figure 6 shows the EDS spectrums of IMCs layer at points A and B as marked in Figure 4.

According to the analysis, the composition of IMCs layer was 69.95% Al, 26.36% Fe and 3.51% Si and 70.55% Al, 13.1% Fe and 12.97% Si at points A and B, respectively.

According to these results and characteristics of typical Al–Fe–Si system, it can be said that the intermetallic phase formed in welded seam side was τ_5 with the chemical formula of $Al_{7.2}Fe_{1.6}Si$ and in steel side, it was θ with the chemical formula of Fe $(Al, Si)_3$.

From past reports [25-27], it has been shown that in the absence of Si element, the binary compound including Fe_2Al_5 and $FeAl_3$ are formed.The formation enthalpy of the IMC layer is one of the key data to predict the formation of the IMC layers. ΔH° is −34, 300 ± 2000 J/mol and -5686 J/mol for $Al_{7.2}Fe_{1.6}Si$ and Fe $(Al)_3$ phases, respectively. So, Si additions can decrease the formation enthalpy of the IMC layers and participate in the IMC layer's formation [25, 28].

4. 2. IMCs Layer Diffusion process controls the growth of IMCs layer. Therefore, Fick's law can calculate it mathematically. Equation (7) has been proposed to calculate the thickness of IMCs layer.

$$d = \sqrt{D \times \Delta t} \tag{7}$$

where d is the thickness of IMCs layer, D is the average of diffusion coefficient of iron into the melted aluminium and Δt is the molten time range. On the other hand, the diffusion coefficient is dependent to temperature and this dependency can be expressed by Arrhenius relation:

$$D = D^{\circ} \exp\left(\frac{-Q}{RT}\right) \tag{8}$$

where $D°$ is the diffusion constant, R is the gas constant, Q is the activation energy for the growth of the IMCs layer and T is the average temperature in the molten time range, as estimated by the FEM thermal analysis [14].

With assumption values of 0.77 m^2/s, 221 kJ/mol, and 8.314 J/mol K for constant coefficients of $D°$, Q, R, respectively [13], and considering Equations (7) and (8), the thickness of IMCs layer can be calculated. As IMCs layer thickness is mostly related to the diffusion of solid iron into melted aluminium alloy, it should be noted that for estimating the average temperature and molten time range, the thermal cycles are considered in a temperature range above 600 °C (Figure 7). Moreover, the assumed values of constant coefficients in this range of temperature are reliable [13, 14].

A comparison between measured and calculated thickness of IMCs layers onto weld heat input has been demonstrated in Figure 8. As can be seen from Figure 8, the thickness of IMCs layer (whether experimentally measured or calculated by FEM simulation and Fick's law) increased with enhancing weld heat input. Moreover, the values experimentally measured, with a slight difference, were higher than those obtained by FEM calculation. It can be said that ignoring the growth of the IMCs layer in the temperature range below 600 °C for the calculated values was a reason for this observation. It can be realized that in higher weld heat input, the difference between the values of measured and calculated IMCs layer thickness was less than that in lower weld heat input (Figure 8).

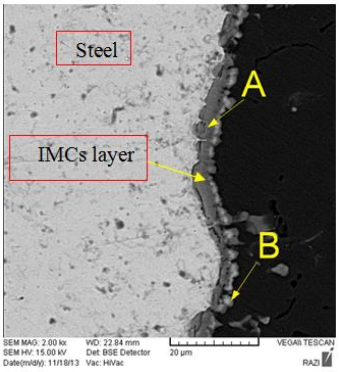

Figure 4. SEM microstructure of the interface between steel and weld seam for sample three

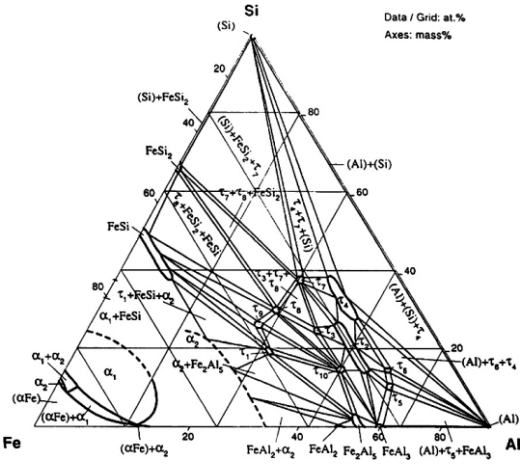

Figure 5. Isothermal section of the Al–Fe–Si system at 600 °C.

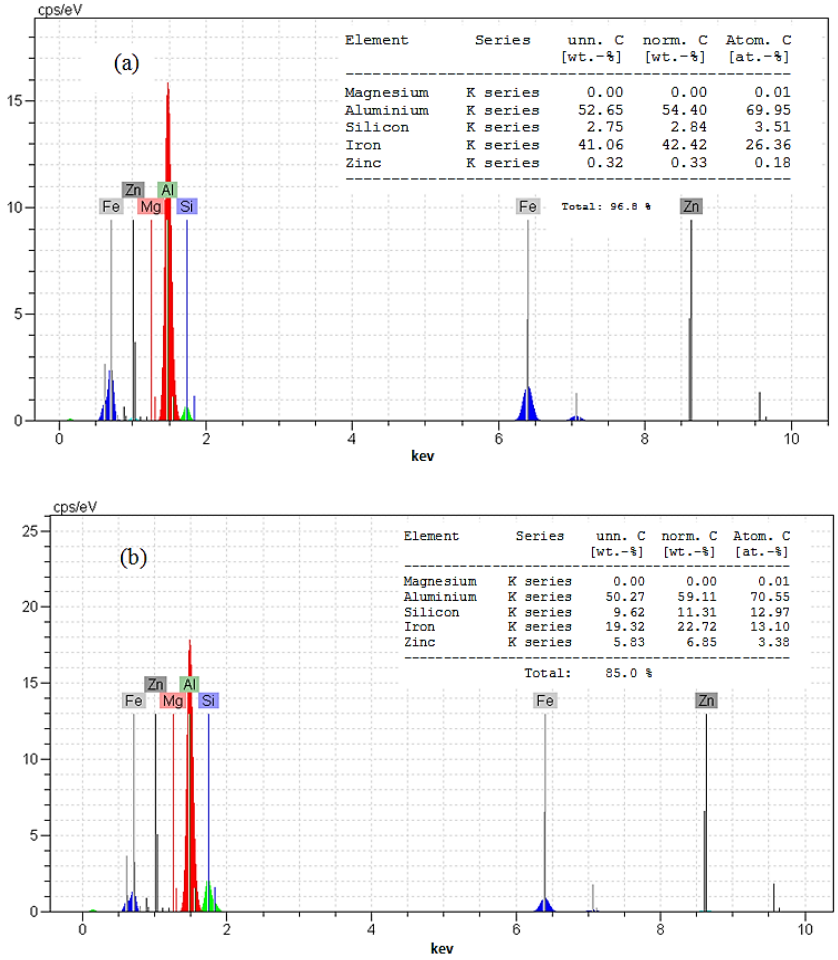

Figure 6. EDS spectrum: compositions of IMCs layer at (a) point A and (b) point B

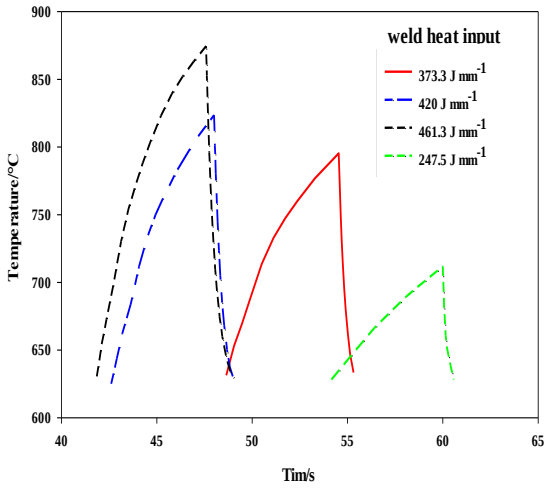

Figure 7. Section of thermal cycles at temperatures above 600 °C.

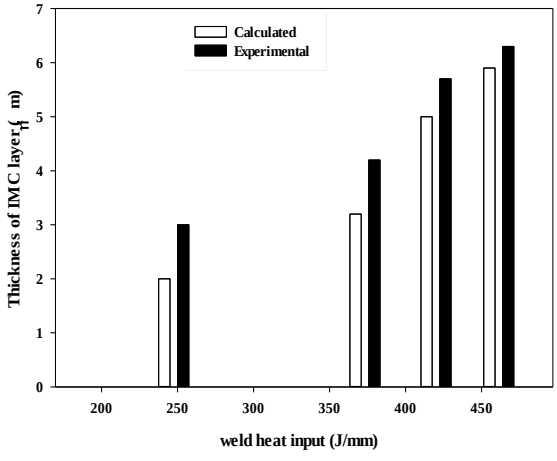

Figure 8. The relation between calculated and measured thickness of IMCs layers under various weld heat inputs.

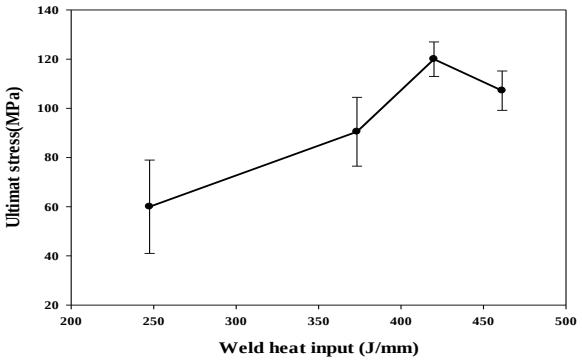

Figure 9. Ultimate stress under various weld heat inputs

4. 3. Mechanical Properties Figure 9 shows the relationship between measured ultimate stress and weld heat input induced by the welding source. The results indicated that in low weld heat input, because of incompatible wetting (incomplete brazing) of steel and incomplete fusion in aluminium side, despite thin IMCs layer, joint strength was low. The increase in heat input led to improving the spreading of the weld metal over the steel surfaces and resolving the incomplete fusion in aluminium side. The highest strength of the joints was received for sample three, reaching to 120 MPa. In this sample, whilst the weld apparent was good, the IMCs thickness was less than the permissible value (10 μm) [8, 9]. The error bar is more wide for sample one, in that the low weld heat input caused poor weldability. As can be seen from Figure 9, increasing weld heat input initially increased the ultimate stress amplitude, but in the weld heat input above 420 J/mm, decreased the value of ultimate stress. The thicker IMCs layer of sample four, compared to sample three, was the reason for its strength degradation.

5. CONCLUDING REMARKS

TIG welding- brazing of 5083 aluminium alloy to galvanised steel with Al-5Si filler wire was evaluated through both FEM numerical simulations and experimental efforts. The effect of weld heat input on the strength properties of joints was investigated. The results of diffusion calculations showed that increasing weld heat input enhanced the thickness of IMCs layer formed at the interface of steel/weld seam, as confirmed by measurements obtained from the microstructures.

The thickness of IMCs layer for whole set welding parameters was 2-6 μm, which was less than the maximum critical value of 10 μm. The IMCs layer near the steel side was Fe $(Al, Si)_3$ and in the weld seam side, it was $Al_{7.2}Fe_{1.6}Si$ and grew towards the fusion weld.

The experimental results indicated that increasing weld heat input improved the brazing of steel and the welding of aluminium. Moreover, the joint pattern with dual characteristics improved the wetting action of the molten weld metal on the steel surfaces. The highest strength of 120 MPa was received for optimized weld heat input of 420 J/mm.

From this paper, it can be said that to reach high strength joint in TIG welding–brazing dissimilar alloy between steel/aluminium, it is necessary to control two factors including thickness of the IMCs layer and spreading of weld metal.

6. REFERENCES

1. Dong, H., Yang, L., Dong, C. and Kou, S., "Improving arc joining of Al to steel and al to stainless steel", ***Materials Science and Engineering: A***, Vol. 534, (2012), 424-435.
2. Dong, H., Yang, L., Dong, C. and Kou, S., "Arc joining of aluminum alloy to stainless steel with flux-cored Zn-based filler metal", ***Materials Science and Engineering: A***, Vol. 527, No. 26, (2010), 7151-7154.
3. Rezaei, G. and Arab, N. B. M., "Investigation on tensile strength of friction stir welded joints in pp/epdm/clay nanocomposites", ***International Journal of Engineering-Transactions C: Aspects***, Vol. 28, No. 9, (2015), 1382-1391.
4. Watanabe, T., Takayama, H. and Yanagisawa, A., "Joining of aluminum alloy to steel by friction stir welding", ***Journal of Materials Processing Technology***, Vol. 178, No. 1, (2006), 342-349.
5. Nikoi, R., Sheikhi, M. and Arab, N. B. M., "Experimental analysis of effects of ultrasonic welding on weld strength of polypropylene composite samples", ***International Journal of Engineering-Transactions C: Aspects***, Vol. 28, No. 3, (2014), 447-453.
6. Liaghat, G., Nouri, M., Darvizeh, A., Al-Hassani, S. and Kormi, K., "Effect of impact parameters on explosive welding of tube to a plug", ***International Journal of Engineering Transaction B: Applications***, Vol. 15, No. 3, (2002), 285-298.
7. Jarry, E. and Shenoi, R., "Performance of butt strap joints for marine applications", ***International Journal of Adhesion and Adhesives***, Vol. 26, No. 3, (2006), 162-176.
8. Lin, S., Song, J., Yang, C., Fan, C. and Zhang, D., "Brazability of dissimilar metals tungsten inert gas butt welding–brazing between aluminum alloy and stainless steel with Al–Cu filler metal", ***Materials & Design***, Vol. 31, No. 5, (2010), 2637-2642.
9. Song, J., Lin, S., Yang, C., Ma, G. and Liu, H., "Spreading behavior and microstructure characteristics of dissimilar metals tig welding–brazing of aluminum alloy to stainless steel", ***Materials Science and Engineering: A***, Vol. 509, No. 1, (2009), 31-40.
10. Su, Y., Hua, X. and Wu, Y., "Influence of alloy elements on microstructure and mechanical property of aluminum–steel lap joint made by gas metal arc welding", ***Journal of Materials Processing Technology***, Vol. 214, No. 4, (2014), 750-755.
11. Dong, H.-g., Hu, W.-j. and Zhang, X.-c., "Detachment of interfacial layers during Arc-brazing of aluminum alloy to carbon steel with filler wire", ***Transactions of Nonferrous Metals Society of China***, Vol. 23, No. 6, (2013), 1583-1588.
12. Chen, S., Li, L., Chen, Y., Dai, J. and Huang, J., "Improving interfacial reaction nonhomogeneity during laser welding–brazing aluminum to titanium", ***Materials & Design***, Vol. 32, No. 8, (2011), 4408-4416.
13. Borrisutthekul, R., Yachi, T., Miyashita, Y. and Mutoh, Y., "Suppression of intermetallic reaction layer formation by controlling heat flow in dissimilar joining of steel and aluminum

alloy", ***Materials Science and Engineering: A***, Vol. 467, No. 1, (2007), 108-113.
14. Fan, J., Thomy, C. and Vollertsen, F., "Effect of thermal cycle on the formation of intermetallic compounds in laser welding of aluminum-steel overlap joints", ***Physics Procedia***, Vol. 12, (2011), 134-141.
15. Lee, C., Chiew, S. and Jiang, J., "Residual stress study of welded high strength steel thin-walled plate-to-plate joints part 2: Numerical modeling", ***Thin-walled Structures***, Vol. 59, (2012), 120-131.
16. Kohandehghan, A. and Serajzadeh, S., "Arc welding induced residual stress in butt-joints of thin plates under constraints", ***Journal of Manufacturing Processes***, Vol. 13, No. 2, (2011), 96-103.
17. Tonkovic, Z., Peric, M., Surjak, M., Garasic, I., Boras, I., Rodic, A. and Svaic, S., "Numerical and experimental modeling of a T-joint fillet welding process", in 11th International Conference on Quantitative Infrared Thermography, Naples Italy., Vol. 250, (2012).
18. Tanner, D. W., "Life assessment of welded inconel 718 at high temperature", University of Nottingham, (2009),
19. Kim, D., Badarinarayan, H., Kim, J. H., Kim, C., Okamoto, K., Wagoner, R. and Chung, K., "Numerical simulation of friction stir butt welding process for AA5083-H18 sheets", ***European Journal of Mechanics-A/Solids***, Vol. 29, No. 2, (2010), 204-215.
20. Bejan, A. and Kraus, A. D., "Heat transfer handbook, John Wiley & Sons, Vol. 1, (2003).
21. Saida, K., Ohnishi, H. and Nishimoto, K., "Fluxless laser brazing of aluminium alloy to galvanized steel using a tandem beam–dissimilar laser brazing of aluminium alloy and steels", ***Welding International***, Vol. 24, No. 3, (2010), 161-168.
22. Jiang, W., Zhang, Y. and Woo, W., "Using heat sink technology to decrease residual stress in 316l stainless steel welding joint: Finite element simulation", ***International Journal of Pressure Vessels and Piping***, Vol. 92, (2012), 56-62.
23. Teng, T.-L., Fung, C.-P., Chang, P.-H. and Yang, W.-C., "Analysis of residual stresses and distortions in T-joint fillet welds", ***International Journal of Pressure Vessels and Piping***, Vol. 78, No. 8, (2001), 523-538.
24. Ma, Z., Wang, C., Yu, H., Yan, J. and Shen, H., "The microstructure and mechanical properties of fluxless gas tungsten arc welding–brazing joints made between titanium and aluminum alloys", ***Materials & Design***, Vol. 45, (2013), 72-79.
25. Song, J., Lin, S., Yang, C. and Fan, C., "Effects of Si additions on intermetallic compound layer of aluminum–steel tig welding–brazing joint", ***Journal of Alloys and Compounds***, Vol. 488, No. 1, (2009), 217-222.
26. Qin, G.-l., Su, Y.-h. and Wang, S.-j., "Microstructures and properties of welded joint of aluminum alloy to galvanized steel by nd: Yag laser+ mig arc hybrid brazing-fusion welding", ***Transactions of Nonferrous Metals Society of China***, Vol. 24, No. 4, (2014), 989-995.
27. Zhang, H. and Liu, J., "Microstructure characteristics and mechanical property of aluminum alloy/stainless steel lap joints fabricated by mig welding–brazing process", ***Materials Science and Engineering: A***, Vol. 528, No. 19, (2011), 6179-6185.
28. Zhang, C.-H., Huang, S., Shen, J. and Chen, N.-X., "Structural and mechanical properties of Fe–Al compounds: An atomistic study by eam simulation", ***Intermetallics***, Vol. 52, No., (2014), 86-91.

Effect of Welding Heat Input on the Intermetallic Compound Layer and Mechanical Properties in Arc Welding-brazing Dissimilar Joining of Aluminum Alloy to Galvanized Steel

M. Zarouni, R. Eslami-Farsani

Faculty of Materials Science and Engineering, K. N. Toosi University of Technology, Tehran, Iran

P A P E R I N F O

Paper history:
Received 02 November 2015
Received in revised form 13 February 2016
Accepted 04 March 2016

Keywords:
Arc Welding-brazing
Numerical Simulation
Dissimilar Alloy
Intermetallic Compound Layer

چکیده

تأثیر حرارت ورودی جوش روی شکل گیری لایه ترکیب بین فلزی در فرآیند جوشکاری لحیم کاری آلیاژ های نامشابه آلومینیم و فولاد، از طریق روش شبیه سازی عددی اجزاء محدود و همچنین اندازه گیری های تجربی، مورد بررسی قرار گرفت. نتایج تحلیل اجزاء محدود و همچنین آزمایش های تجربی نشان داد که افزایش دادن حرارت ورودی جوش، ضخامت لایه بین فلزی را افزایش می‌دهد. اندازه ضخامت لایه های بین فلزی محاسبه شده از شبیه سازی های اجزاء محدود، تقریباً با مقادیر اندازه گیری شده از تصاویر میکروسکوپی برابر بود و در یک رنج ٦-٢ میکرومتری قرار داشت. استحکام کششی اتصال های جوشکاری- لحیم کاری، به ضخامت لایه بین فلزی و پخش‌شدگی فلز مذاب روی سطوح فولاد بستگی داشت. بالاترین استحکام مکانیکی (۱۲۰ مگاپاسکال) در حرارت ورودی بهینه ٤٢٠ ژول بر میلی‌متر، بدست آمد. وجود عنصر سیلیسیم در فلز پرکننده آلومینیم- سیلیسیم با نسبت اتمی ۵/۹۵، منجر به ایجاد لایه بین فلزی با ترکیب شیمیایی فاز آهن- (آلومینیم، سیلیسیم) با نسبت اتمی ۳/۱ در طرف فولاد، و فاز آلومینیم- آهن- سیلیسیم با نسبت اتمی ۱۰/۱٦/۷۲ در طرف فلز جوش شد.

***doi**: 10.5829/idosi.ije.2016.29.05b.11*